Positron annihilation study of the electronic structure of LaB_6 and CeB_6

M. Biasini,* H. M. Fretwell, S. B. Dugdale, and M. A. Alam
H.H. Wills Physics Laboratory, University of Bristol, Tyndall Avenue, Bristol BS8 1TL, United Kingdom

Y. Kubo
Department of Physics, College of Humanities and Sciences, Nihon University, Tokyo 156, Japan

H. Harima
CIAS, University of Osaka Prefecture, Sakai, Osaka 593, Japan

N. Sato
Department of Physics, Tohoku University, Aramaki Aoba, Sendai 980-77, Japan
(Received 27 June 1996; revised manuscript received 6 May 1997)

We measured the two-dimensional angular correlation of the positron annihilation radiation (2D-ACAR) on a single crystal of LaB_6 for two projections. The anisotropies of the 2D electron-positron momentum density were very similar to those observed for the isostructural heavy-fermion (HF) system CeB_6 in the paramagnetic phase and consistent with those of the calculated electron-positron momentum density of LaB_6. The standard Lock-Crisp-West (LCW) analysis was in reasonable agreement with the LCW folding of the calculated 2D-ACAR spectrum and the de Haas–van Alphen findings. From the projected $\boldsymbol{k}$-space density we could evaluate the Fermi volume, corresponding to 1.10 ± 0.04 electrons per formula unit, and deduce that the effect of the nonuniform positron density does not play a significant role. The apparent discrepancy with the LCW analysis of CeB_6, where filtering procedures were required to recover a $\boldsymbol{k}$-space density similar to that obtained for LaB_6, is discussed. [S0163-1829(97)02339-4]

I. INTRODUCTION

The compound LaB_6 is the reference non-f-electron paramagnetic metal, isostructural to the heavy-fermion (HF) hexaboride CeB_6 which is notable for its nonstandard HF behavior. In CeB_6 the Ruderman-Kittel-Kasuya-Yosida (RKKY) indirect exchange interaction competes with the Kondo effect to produce a complex low-temperature magnetic phase diagram with an antiferromagnetic ordering at the Néel temperature $T_N=2.3$ K.[1,2] Therefore, the low-temperature behavior of CeB_6 [as for other HF's, such as $CePd_2Al_3$ and CePdAl (Refs. 3, 4)] differs from that of standard HF systems such as $CeAl_3$ and $CeRu_2Si_2$ which are better understood. In these systems the hybridization and consequent formation of the Kondo singlets between f electrons and conduction electrons leads to the washout of the $4f$ electron magnetic moment below the Kondo temperature T_K.[5] Very narrow bands pinned at the Fermi level (E_F) then produce a high density of states near E_F and account for the high value of the low-temperature specific heat and cyclotron masses observed, at $T\ll T_K$, by thermodynamic and quantum oscillation experiments.[6] Conversely, in the case of CeB_6, it appears that the Kondo singlet formation coexists with the magnetic ordering. The absence of a paramagnetic ground state raises a question regarding the itinerant or localised character of the f electrons in CeB_6. The de Haas van Alphen (dHvA) and acoustic dHvA measurements, performed at $T<T_K$,[7–11] yielded similar Fermi surface (FS) features for CeB_6 and LaB_6, suggesting that the f electrons might not contribute to the Fermi volume. However, these measurements were performed under application of strong magnetic fields B which perturb the coherent Kondo lattice ground state when $k_BT_K\ll\mu B$ (where μ is the saturation magnetic moment of CeB_6, $\mu\simeq1\mu_B$, and, following Sato *et al.*,[12] $T_K\simeq1-2$ K). The dHvA measurements on CeB_6 were confirmed in the paramagnetic phase (at $T>T_K$) by two-dimensional angular correlation of the positron annihilation radiation (2D-ACAR) experiments, where filter procedures were utilized to separate the FS signals from other structures present in the spectra.[13] Previous 2D-ACAR experiments of LaB_6 (Ref. 14) showed discrepancies with dHvA data and theory which were only partially solved by further measurements yielding 3D reconstructed momentum data.[15]

We performed experiments on this compound to compare the FS results with those obtained for CeB_6. Other candidate mechanisms generating the low-temperature HF behavior in the absence of the invoked weak hybridisation are currently being discussed. It is therefore worth confirming the similarities of the FS's of the two compounds via the 2D-ACAR technique which, unlike dHvA, is not restricted to experiments at very low temperatures ($T<1$ K) and high magnetic fields ($B>10$ T).

The 2D-ACAR experiment determines a two-dimensional projection or integral of the two-photon electron-positron momentum density $\rho^{2\gamma}(\boldsymbol{p})$ which, in the independent particle model (IPM), can be expressed (in atomic units) as

$$\rho^{2\gamma}(\boldsymbol{p})=\text{const}\times\sum_{n,\boldsymbol{k}}^{\text{occ}}\left|\int\exp(-i\boldsymbol{p}\cdot\boldsymbol{r})\,\psi_{\boldsymbol{k}}^{n}(\boldsymbol{r})\,\phi(\boldsymbol{r})\,d\boldsymbol{r}\right|^2. \tag{1.1}$$

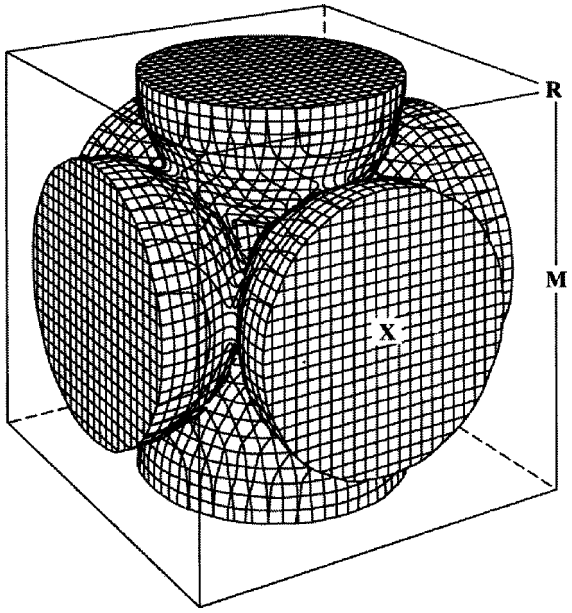

FIG. 1. The multiply connected ellipsoidal Fermi surfaces of LaB_6. The circular cross section of the ellipsoids is normal to the Γ-X direction. The ellipsoid radii assumed were 32% and 41% of the BZ for the X-M and Γ-X directions, respectively. The Γ point (not seen) is at the center of the BZ.

Here $\psi_{\boldsymbol{k}}^n$ and ϕ denote the electron and positron wave function, respectively, and the summation extends over all occupied $\boldsymbol{k}$ electron states from bands of index n.

For periodic systems, $\rho^{2\gamma}(\boldsymbol{p})$ is discontinuous at points $\boldsymbol{p}_F=(\boldsymbol{k}_F+\boldsymbol{G})$, where $\boldsymbol{G}$ is a reciprocal lattice vector and $\boldsymbol{k}_F$ is the reduced Fermi wave vector in the first Brillouin zone (BZ). When the FS discontinuities are distributed over many BZ and superimposed on a high intensity smooth background contributed by the valence bands, the standard Lock-Crisp-West (LCW) analysis is often usefully employed.[16] This procedure consists in folding the momentum distribution $\rho^{2\gamma}(\boldsymbol{p})$ back onto the first BZ by translation over the appropriate reciprocal lattice vectors. In the IPM, the result, $\rho_{\mathrm{LCW}}(\boldsymbol{k})$, is the electron occupation number modulated by the overlap integral of the $\boldsymbol{k}$ electron and the positron density[17]

$$\rho_{\mathrm{LCW}}(\boldsymbol{k})=\mathrm{const}\times\sum_n\ \theta(E_F-\epsilon_{k,n})\times\int|\psi_k^n(\boldsymbol{r})|^2|\phi(\boldsymbol{r})|^2d\boldsymbol{r}, \tag{1.2}$$

where $\epsilon_{k,n}$ is the energy eigenvalue of the $|\psi_k^n\rangle$ eigenstate. The procedure is particularly effective when the overlap integral in Eq. (1.2) is large and weakly $\boldsymbol{k}$ dependent and if the electron-positron correlations are independent of $\boldsymbol{k}$ too. In this paper the anisotropies of the experimental angular-correlation spectra of LaB_6, $\rho^{2\gamma}(\boldsymbol{p})$, are compared with those of the CeB_6 spectra measured in our work of Ref. 13 and with those of the calculated electron-positron momentum density. The Fermi volume is assessed via a simple processing of the LCW folded data. Moreover, the results of the LCW analysis are discussed in relation to the corresponding findings on CeB_6.

II. EXPERIMENTAL DETAILS

The LaB_6 single crystal was grown by the floating zone method. Detailed description and characterization are reported elsewhere.[12] The 2D-ACAR experiments were performed on the Bristol-Bologna spectrometer,[13] having angular resolution (for a point-source) of 0.57 mrad (1 milliradian is equivalent to 0.137 momentum a.u.) and resolving coincidence time for photon pair selection of 60 nsec. The estimated overall experimental resolution, obtained by combining the angular resolution with the intrinsic sizes of the positron-source spot at the sample and the thermal motion of the positron ($\sim$0.15 mrad, at 30 K), was (0.59, 0.73) mrad for the p_x and p_y directions, respectively (10% and 12% of the BZ size of LaB_6). Data were accumulated in a (288×288) matrix with a bin size of (0.135×0.135) mrad^2. It is well known[18] that a 2D-ACAR experiment determines the two-dimensional (2D) projection $\rho_{2\mathrm{D}}^{2\gamma}(p_x,p_y)$ of the electron-positron momentum distribution $\rho^{2\gamma}(\boldsymbol{p})$ by measuring the distribution $N(\theta_x,\theta_y)$ of the deviation angles from anticollinearity of the annihilation γ rays:

$$N(\theta_x,\theta_y)=\mathrm{const}\times\rho_{2\mathrm{D}}^{2\gamma}(p_x,p_y)=\mathrm{const}\times\int_{-\infty}^{\infty}\rho^{2\gamma}(\boldsymbol{p})dp_z, \tag{2.1}$$

where the average integration direction p_z is specified by the detector-sample-detector axis of the spectrometer.

We performed two measurements, at the temperature of $\sim$30 K and pressure of 5×10^{-6} Torr. The first, with integration along the $\langle100\rangle$ direction of the crystal to a total $\simeq2\times10^8$ coincidence counts. Because of experimental problems encountered, the second projection, along the $\langle110\rangle$ axis, had to be stopped at 3×10^7 counts. The two ''raw'' spectra were subsequently corrected with the so-called momentum sampling function, which removes the distortions resulting from spatial variations in the single detector efficiencies and the finite apertures of those detectors.[19] After ensuring that the anisotropy of the raw data had a natural symmetry compatible with the symmetry axes p_x and p_y of the spectrometer, the spectra [in the following denoted as (100) and (110) projections] were finally symmetrized, i.e., folded about the relevant crystal symmetry axes to further enhance the statistics.

III. RESULTS AND DISCUSSIONS

The unit cell of all the rare earth hexaborides (RB_6), is simple cubic:[20] it contains an R atom and a regular octahedron of six B atoms. The early augmented-plane-wave (APW) band structure calculations of Hasegawa *et al.*[20] yielded for LaB_6 a rather simple FS topology. This consists of a set of nearly symmetrical electron ellipsoids centred at the X points (of the simple cubic BZ) and connected by thick necks along the $\Gamma-M(\Sigma)$ axes. The conduction band exhibits a strong $\boldsymbol{k}$ dispersion generating band masses which are lighter than the free electron mass m_0, and in agreement with experimental results of the cyclotron masses m^* ($m^*\simeq0.6m_0$,[9]). A second FS sheet of 12 smaller electron pockets (located along the Σ axes), detected by acoustic dHvA measurements,[21,10] is disregarded here because their

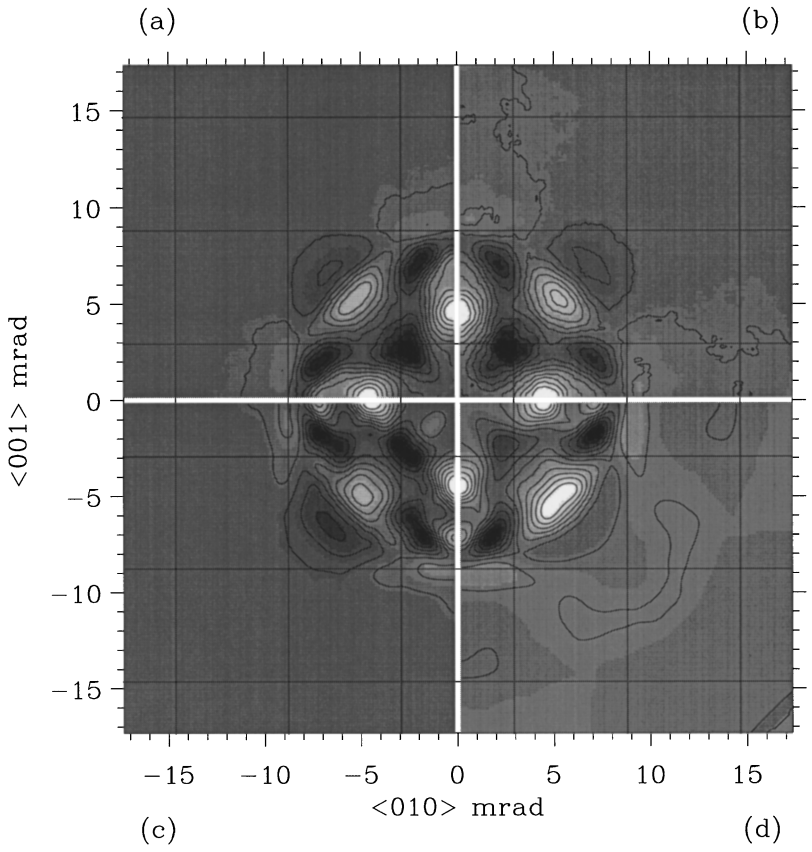

FIG. 2. (a) Radial anisotropy (RA) of the measured and symmetrized (see text) two-photon momentum distribution $\rho^{2\gamma}(\boldsymbol{p})$ of LaB_6 for integration along the $\langle 100\rangle$ direction. The spectrum was smoothed with an equally weighted smoothing array of (0.67×0.67) mrad^2 (1 mrad=0.137 a.u.). The borders of the projected first BZ in a repeated zone scheme are shown in (a)–(d). In this and all following gray scale figures, white corresponds to high intensity and black to low intensity. (b) Same as (a) for CeB_6 (from Ref. 13). (c) RA of the theoretical electron-positron $\boldsymbol{p}$-space density for LaB_6, $\rho^{LaB_6}(\boldsymbol{p})$, integrated along the $\langle 100\rangle$ direction and convoluted with the experimental resolution (Ref. 24). (d) RA of the theoretical $\rho_{f\ \mathrm{core}}^{CeB_6}(\boldsymbol{p})$ for CeB_6 (see text), integrated along the $\langle 100\rangle$ direction and convoluted with the experimental resolution (Ref. 25).

sizes are much lower than the limit set by the resolution of the spectrometer.

Figure 1 shows a regular prolate ellipsoids' FS model. Ellipsoid sizes were adopted from acoustic dHvA measurements of LaB_6.[10]

In the 2D-ACAR analysis it has become common practice to highlight the anisotropy of the spectra by displaying the difference between the spectra and their angular average.[22] This difference, denoted as radial anisotropy (RA), gives information on the FS topology whenever the anisotropy of the total electron-positron momentum density $\rho^{2\gamma}(\boldsymbol{p})$ is mainly caused by the discontinuities of the momentum density of the conduction band at the $\boldsymbol{k}_F+\boldsymbol{G}$ points. These discontinuities occur along directions which have the BZ, rather than the radial symmetry.

The maximum amplitudes of the RAs in the twice-folded (100) and (110) projections were 3.9 and 5.7% of the maxima respectively, corresponding to ~ 15 times and ~ 9 times the statistical uncertainty of these maxima. To elucidate the role played by the f electrons in heavy-fermion systems, it is worth comparing the RA's of the LaB_6 spectra with those of CeB_6 reproduced from Ref. 13. Figures 2(a), 2(b), 3(a), and 3(b) show the resulting RA parts of the (100) and (110) projections for LaB_6 and CeB_6, respectively. The RA's of the spectra display a very similar structure in the corresponding projections. In particular, one can ascertain that in the (100) projection [Figs. 2(a) and 2(b)] the common structures of the experimental RA's consisting of the minima at the corners of the first BZ at (2.5, 2.5) mrad, the maxima at (4.5, 0) mrad and at (5.5, 5.5) mrad are related to the FS topology of LaB_6. This could be inferred by constructing a simple simulation of the momentum density whose anisotropy was generated solely by the topology of the FS calculated in Ref. 21. The simulated spectrum, presented by these authors in Ref. 13, is not reproduced here.

The electron-positron momentum density [Eq. (1.1)] of LaB_6 [denoted by $\rho^{LaB_6}(\boldsymbol{p})$] was calculated by Kubo *et al.* adopting the full-potential linearized-augmented-plane-wave method (FLAPW) in local-density approximation (LDA) for the band structure calculation. Details of the computational method are described in Refs. 23, 24. The standard LDA calculation was also adopted to produce the electron-positron momentum density of CeB_6 [denoted by $\rho_{f\ \mathrm{band}}^{CeB_6}(\boldsymbol{p})$].[23,24] The resulting FS, generated by bands of mostly $4f$ character, was in poor agreement with the dHvA measurements mentioned in Sec. I. It is generally accepted that the inappropriate description of many-body effects causes standard LDA calcu-

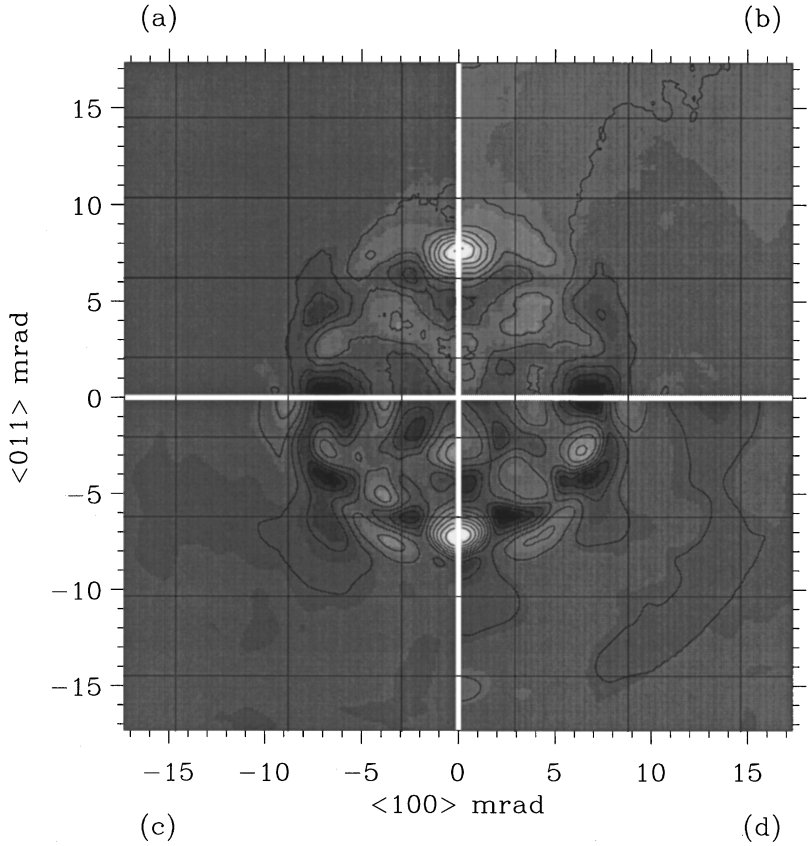

FIG. 3. (a) Radial anisotropy (RA) of the measured and symmetrized (see text) two-photon momentum distribution $\rho^{2\gamma}(\boldsymbol{p})$ of LaB_6 for integration along the $\langle 110\rangle$ direction. Owing to the poorer statistics, the sizes of the smoothing array were increased to (0.9×0.9) mrad^2. The borders of the projected first BZ in a repeated zone scheme are shown in (a)–(d). (b) Same as (a) for CeB_6 (from Ref. 13). (c) RA of the theoretical electron-positron $\boldsymbol{p}$-space density for LaB_6, $\rho^{LaB_6}(\boldsymbol{p})$, integrated along the $\langle 110\rangle$ direction and convoluted with the experimental resolution (Ref. 24). (d) RA of the theoretical $\rho_{f\ \mathrm{core}}^{CeB_6}(\boldsymbol{p})$ for CeB_6, (see text) integrated along the $\langle 110\rangle$ direction and convoluted with the experimental resolution (Ref. 25).

lations to yield f-band widths which lead to underestimated values of the low-temperature specific heat and do not account for the high extent of localization of the $4f$ electrons. The related electron-positron momentum density (not shown here) showed noticeable discrepancies with the experimental results too. A different band structure calculation[25] (denoted as the f-core model) followed the application of the standard rare-earth-like description, where the $4f$ states are regarded as partially filled corelike states. The electron-positron momentum density [denoted by $\rho_{f\ \mathrm{core}}^{CeB_6}(\boldsymbol{p})$] was produced accordingly. The calculations of Kubo *et al.*[23–25] did not include the contribution from the inner shells and neglected a $\boldsymbol{k}$-dependent electron-positron overlap enhancement.

Figure 2(c) shows the RA of the calculated electron-positron momentum density of LaB_6, $\rho^{LaB_6}(\boldsymbol{p})$, for the (100) projection, after integration along the experimental projection direction and the convolution with the assumed resolution function. It appears that all the major structures present in the experimental RA's which were addressed above as FS signatures in Figs. 2(a) and 2(b) [i.e., the minima at (2.5, 2.5) mrad, the maxima at (4.5, 0) and (5, 5) mrad], are accounted for by the electron-positron theory. The same structures are reflected in the RA of the corresponding projection of the $\rho_{f\ \mathrm{core}}^{CeB_6}(\boldsymbol{p})$ calculation, shown in Fig. 2(d), after the convolution with the assumed resolution function. The $\rho_{f\ \mathrm{core}}^{CeB_6}(\boldsymbol{p})$ calculation contains some discrepancy with its experimental counterpart [compare Figs. 2(b) and 2(d)] which consists of the softer minima at (2.5, 2.5) mrad and (7, 7) mrad. However, the overall agreement with the experiments is much better than that shown by the $\rho_{f\ \mathrm{band}}^{CeB_6}(\boldsymbol{p})$ calculation mentioned above. In Fig. 3 [showing the (110) projections] one can notice good agreement between experiments and calculations in the maxima at (0,7.5) mrad and minima at (6.5, 0) mrad, which were attributed to electron momentum wave-function anisotropies.[13] The agreement is less pronounced for the other structures present in the spectra. However, the low statistical precision of the experimental data prevents a detailed analysis of these structures.

From a general point of view, the strong similarities of the experimental anisotropies of LaB_6 and CeB_6 support the hypothesis that the f electrons of CeB_6, at $T>T_K$, can be considered as part of the ion cores.[5,6] In this regard, it is worth pointing out that recent photoemission experiments on other Ce-based HF compounds[26,27] have obtained opposite results, showing that the itinerant character of the $4f$ electrons can remain at $T>T_K$. In the light of those measurements it appears that the localisation of the f electrons at $T>T_K$, shown by CeB_6, should not be viewed simply as reflecting the standard HF behavior, but as a consequence of its low temperature magnetic ordering.

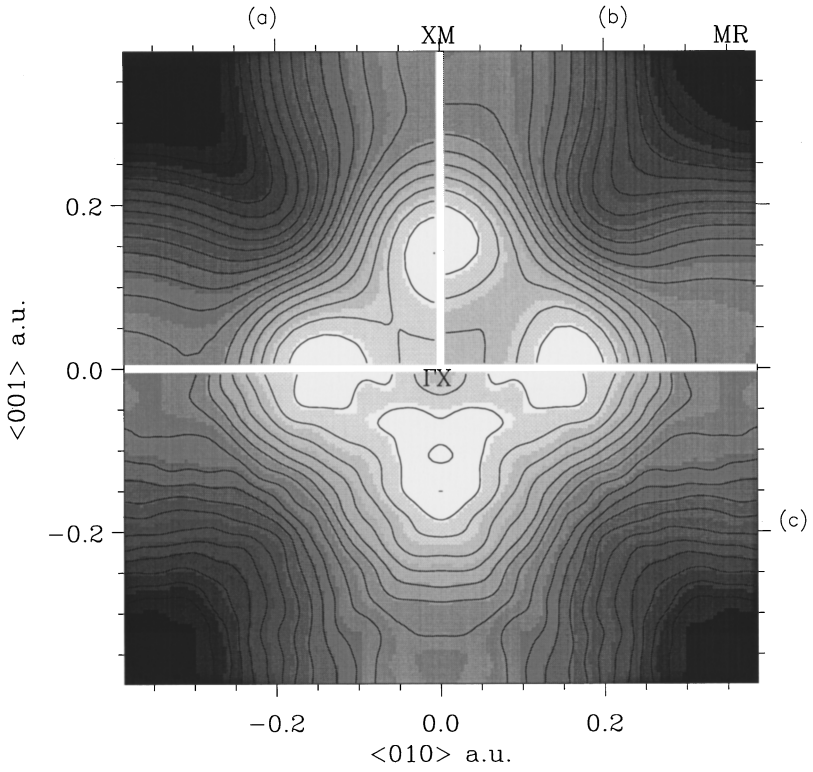

FIG. 4. Upper part: Theoretical ***k***-space density for LaB_6 integrated along the ⟨100⟩ direction and convoluted with the asymmetric experimental resolution. (In Figs. 4–6 the ***k***-space densities are shown in the first BZ.) (a) Electronic occupancy (Ref. 21). (b) Calculated IPM $e^+ - e^-$ ***k***-space density (Ref. 24). Lower part: (c) Experimental LCW ***k***-space density for the same projection. Smoothing=(0.04×0.04) a.u.^{2}. Momentum data were twice folded (see text). The labeling describes the projected BZ high symmetry points.

Figures 4, 5, and 6 show the standard LCW folding in the first BZ for the (100) and (110) projections of LaB_6. In the case of the (100) projection, the experimental LCW data [denoted by LCW_{100} and shown in Fig. 4(c)] are compared to the the projected electronic occupancy (from the main ellipsoidal FS), as calculated by Harima *et al.*[21] and with the electron-positron ***k***-space density, as described by Eq. (1.2), of Kubo *et al.*[23,24] [obtained by LCW folding $\rho^{LaB_6}(\boldsymbol{p})$ and denoted by LCW^{th}_{100}]. The two ***k***-space calculations are shown in Figs. 4(a) and 4(b), after the integration along the experimental projection direction and the convolution with the assumed resolution function. Both calculations used the FLAPW method in LDA. In the calculation by Harima *et al.*,[21] the second small FS sheet mentioned above, which gives negligible contribution to the occupancy after the convolution with the resolution function, was obtained by displacing the $4f$ level upward by 0.1 Ry. The main ellipsoidal FS was essentially unaffected by the displacement. Therefore, apart from the effect of the nonuniform positron density, the two calculations are equivalent. The clear similarity between Figs. 4(a) and 4(b) indicates that the positron distortion of the calculated ***k***-space electron density has marginal effect. A further comparison between data and theory is facilitated by showing, in Fig. 5, the two high symmetry slices of the (100) occupancy, XM-ΓX-XM and MR-XM-MR for the LCW_{100} experiment and the LCW^{th}_{100} theory of Kubo *et al.*[23,24] after the subtraction of the minimum from LCW_{100} and LCW^{th}_{100} and the normalization of LCW^{th}_{100} to LCW_{100}. It is worth realizing that in the (100) projection of the electronic occupancy the intensity of the four maxima surrounding the ΓX point [at $\sim(0.15,\ 0)$ a.u.], arising from the extent of the necks of the ellipsoidal FS, coincides with the size of the BZ, apart from the smearing effect of the experimental resolution.

As Figs. 4 and 5 show, the agreement between data and theory is rather satisfactory. However, the total amplitude

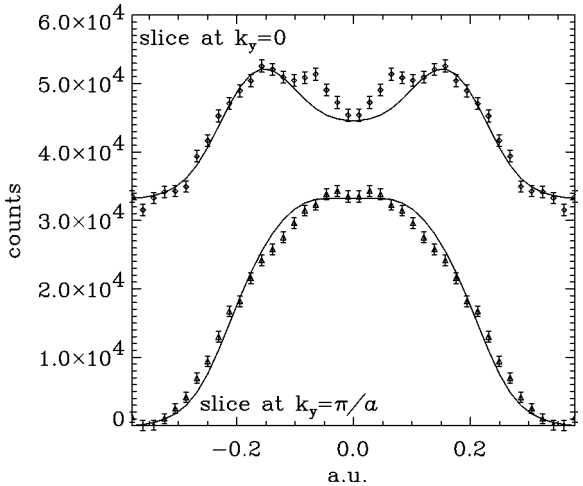

FIG. 5. The cuts of the experimental LCW_{100} [from Fig. 4(c), after a further symmetrization along the ⟨110⟩ axis] at $k_y=0$ (central) and $k_y=\pi/a$ (border) of the BZ, are compared with the corresponding slices from the LCW^{th}_{100} theory shown in Fig. 4(b) (continuous lines).

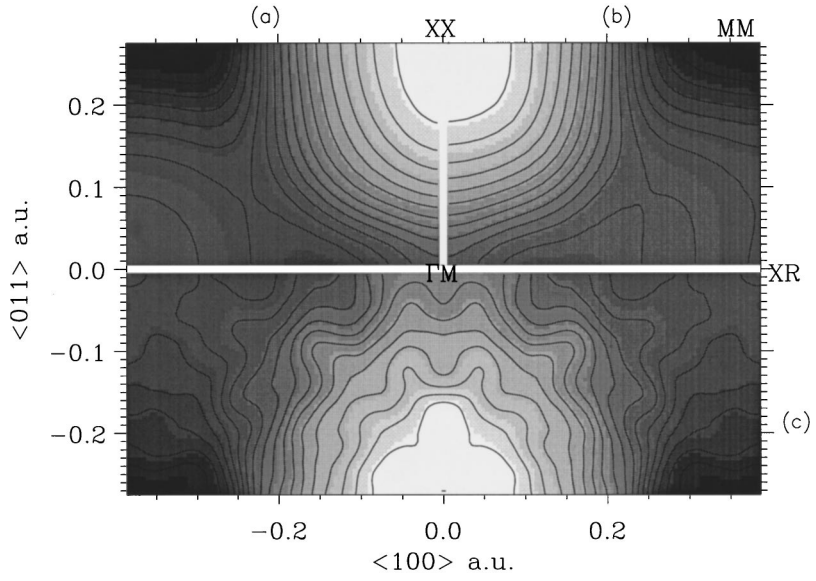

FIG. 6. Upper part: Theoretical $\boldsymbol{k}$-space density for LaB_6 integrated along the $\langle 110 \rangle$ direction and convoluted with the asymmetric experimental resolution. (a) Electronic occupancy (Ref. 21). (b) Calculated IPM $e^+ - e^-$ $\boldsymbol{k}$-space density (Ref. 24). Lower part: (c) Experimental LCW $\boldsymbol{k}$-space density for the same projection direction. Smoothing$=(0.04\times0.04)$ a.u.^{2}. The labeling describes the projected BZ high symmetry points.

variation of the experimental LCW_{100} matrix is 4.7%, equivalent to ~ 45 times the average statistical error of the LCW_{100} intensity (for the twice folded data), as opposed to 6.6%, of the LCW^{th}_{100} theory. Another discrepancy between experiment and theory, shown in Fig. 5, arises from the satellite structures at $\sim(0.07,\ 0)$ a.u., located between the maxima due to the necks of the ellipsoidal FS and the center of the LCW_{100} matrix. The satellite peaks are present in both the k_x and k_y directions (although they are of different intensities) prior to the symmetrization about the $\langle 110 \rangle$ axis performed when showing Fig. 5. Therefore, they cannot be due to experimental artifacts or symmetrized noise. We have no explanations for these discrepancies. The LCW^{th}_{100} calculation neglects the electron-positron correlation. However, it is unlikely that the sharp structures noted above can be ascribed to a strongly $\boldsymbol{k}$-dependent enhancement of the overlap integral present in Eq. (1.2).[28]

As suggested by the similarities of LCW^{th}_{100} [Fig. 4(a)] and the calculated projected electronic occupancy [Fig. 4(b)], we evaluated the Fermi volume under the assumption of a constant positron wave function. In this case, the contribution of the full bands is constant (here consisting of the minimum of the LCW_{100} matrix). The following steps can then be performed.

(1) Subtract the minimum from the LCW_{100} folded data.

(2) Rescale LCW_{100} so that the intensity of the four maxima surrounding the ΓX point represents the size of the BZ modulated by the smearing effect of the experimental resolution function (with our setup those maxima are decreased to 96% of their original value). The rescaling factor is, therefore, the ratio of the ''decreased'' size of the BZ to the value obtained by fitting the experimental maxima with a Gaussian (to avoid scatter due to noise and artifacts).

(3) Compute the ratio R of the total number of counts in the rescaled matrix to the volume of the BZ.

The obtained ratio is $R = 0.55 \pm 0.02$. The same procedure applied (as a test of consistency) to the LCW^{th}_{100} data[25] and the projected electronic occupancy,[21] yielded ratios of 0.53 and 0.49, respectively. Owing to the simplicity of the topology of LaB_6's FS this result can be interpreted immediately: only one band crosses the Fermi level (the contribution of the small electron pockets to the Fermi volume is negligible, being less than 10^{-4} of the BZ volume). As LaB_6 is an uncompensated metal the only conduction band is semioccupied. The Fermi volume obtained by this analysis corresponds to 1.10 ± 0.04 electrons under the assumption of spin degeneracy. Its relatively small departure from the ideal value suggests that in LaB_6 the positron wave function does not play a significant role and supports a theory (LCW^{th}_{100}) yielding results not dissimilar to those of a purely electronic occupancy.

Figures 6(a) and 6(b), show the projected electron occupancy[21] and the projected electron-positron calculation[24] after the convolution with the experimental resolution. Figure 6(c) shows the result of the LCW procedure for the (110) projection of LaB_6. The total amplitude variation of the experimental $\boldsymbol{k}$-space density is 3.7%, equivalent to ~ 16 times the average statistical error of the intensity (for the twice folded data). Within the limits of the lower statistical precision, the agreement between data and both theories is again quite satisfactory.

In our work of Ref. 13 the application of the standard LCW transformation to the CeB_6 momentum data highlighted a poor agreement between the experimental data and the predictions of the electronic structure suggested by the f-core model,[25,29] which yields essentially the same FS for CeB_6 and LaB_6. The discrepancy between experiment and theory was particularly evident in the case of the (100) projection. We conjectured that the difference between experimental $\boldsymbol{k}$-space density and theoretical projected occupancy was due to the the modulation in $\boldsymbol{k}$ space generated by a nonuniform positron density and applied new filtering

procedures.[13] Since none of this filtering was required in the analysis of LaB_6, this explanation seems now less likely. In this case, the positron wave-function effect introduced only a relatively small perturbation to the electronic occupancy. In this regard, one should realize that the condition of a constant positron wave function, which simplifies the result of Eq. (1.2) to the electronic occupancy and is unrealistic because the positron resides prevalently in the interstices, could be relaxed to the condition that the overlap integral in Eq. (1.2) is independent of k and n. The fact that in LaB_6 only one band crosses the Fermi level and that the conduction electrons are highly delocalized (as shown by their small effective mass[9,21]) favors the recovery of the true occupancy. Moreover, as the f band is very narrow, a strongly $\boldsymbol{k}$-dependent overlap integral between the f electrons and the positron densities in CeB_6 cannot be explained. In fact, the LCW folding of the calculated electron-positron momentum density of CeB_6 via the f-core model $\rho_{f\ \mathrm{core}}^{\mathrm{CeB_6}}(\boldsymbol{p})$, yields a $\boldsymbol{k}$-space density (not shown) almost identical to the electronic occupancy of LaB_6.

The evidence that the RA's of the two compounds' momentum spectra were very similar and their good agreement with the RA's of the theoretical momentum densities of $\rho^{\mathrm{LaB_6}}(\boldsymbol{p})$ and $\rho_{f\ \mathrm{core}}^{\mathrm{CeB_6}}(\boldsymbol{p})$, suggests that some additional radially symmetric contribution, independent of the FS of the compounds, is present in the spectra of CeB_6.[30] We considered the possibility that this contribution was related to defects in the CeB_6 sample and performed positron lifetime experiments on the two compounds. As in both cases only one single crystal was available, the lifetime experiment, in the usual sandwich configuration, was performed with the LaB_6 (CeB_6) single crystal on one side of the ^{22}Na source (deposited between two Kapton foils) and a well annealed aluminium sample on the other side. The several exponential components present in the spectra reduced the effectiveness of the fitting procedure. The lifetime results, consistent with previous (unpublished) measurements of LaB_6,[31,32] will be reported elsewhere. Here we note that, within the level of accuracy of the experiment described, the lifetime analysis did not resolve in CeB_6 extra-lifetime components which could be ascribed to defects.

To resolve the issue measurements on CeB_6 were performed by Manuel *et al.*[32] The results will be published elsewhere. Here we anticipate that, whereas the anisotropies of the momentum spectra confirmed fully the results reported here, the LCW-folded data showed a good agreement with the predictions of the f-core calculation without the need of the filtering which was applied in Ref. 13.

On completion of the measurements of CeB_6[13] the picture which could be drawn from our experiments was that, at 30 K, i.e., in the paramagnetic phase, the observed momentum distribution and the related $\boldsymbol{k}$-space densities were consistent with theoretical models of the Fermi surface obtained by treating the f electrons as localized. This conclusion was reached under the assumption that the adopted filter procedure (denoted as *band pass*) was primarily eliminating the effect of a nonuniform positron density from the momentum data. The further measurements on LaB_6, the calculations of the electron-positron momentum density of CeB_6, $\rho_{f\ \mathrm{core}}^{\mathrm{CeB_6}}(\boldsymbol{p})$, and the measurements on CeB_6 (Ref. 32) indicate that the contribution which in CeB_6 was filtered by the band-pass procedure[13] cannot be ascribed to a positron effect but support our previous conclusions regarding the role played by the $4f$ electrons in CeB_6.

IV. CONCLUSION

We have performed 2D-ACAR experiments on a single crystal of LaB_6 for two integration directions. The anisotropies of the angular-correlation spectra and the LCW folded $\boldsymbol{k}$-space densities confirm to a large extent the FS topology detected by the quantum oscillation experiments and calculated via the standard LDA. The anisotropies of the measured spectra are very similar to those of the isostructural heavy-fermion system CeB_6 in the paramagnetic phase observed in our previous experiments.[13] The anisotropies of the CeB_6 spectra show very good agreement with those of calculations of the electron-positron momentum spectra where the Ce $4f$ electrons are regarded as corelike states. These findings support the supposition that, at $T > T_K$, the $4f$ electrons of HF systems undergoing magnetic ordering are conveniently modelled by atomic levels with associated localized magnetic moments.[5,6]

ACKNOWLEDGMENTS

We gratefully thank Dr. A. Manuel for sending us the results of the experiments on CeB_6 prior to publication. We are indebted to Dr. J. Kaiser for his software contribution and to Professor R. West for stimulating discussions. This work was supported by EPSRC (U.K.), INFM (Italy), ENEA (Italy), and the Royal Society (U.K.).

*Permanent address: ENEA, Via Don Fiammelli 2 40129 Bologna, Italy.

[1] M. Effantin, J. Rossat-Mignod, P. Burlet, H. Bartholin, S. Kunii, and T. Kasuya, J. Magn. Magn. Mater. **47 & 48**, 145 (1985).

[2] S. Nakamura, T. Goto, and S. Kunii, J. Phys. Soc. Jpn. **64**, 3941 (1995).

[3] H. Kitazawa, C. Schank, S. Thies, B. Seidel, C. Geibel, and F. Steglich, J. Phys. Soc. Jpn. **61**, 1461 (1992).

[4] H. Kitazawa, A. Matsushita, T. Matsumoto, and T. Suzuki, Physica B **199-200**, 28 (1994).

[5] P. Fulde, J. Low Temp. Phys. **95**, 45 (1994).

[6] F. Steglich, C. Geibel, K. Gloos, G. Olesch, C. Schank, C. Wassilew, A. Loidl, A. Krimmel, and G. R. Stewart, J. Low Temp. Phys. **95**, 3 (1994).

[7] Y. Ishizawa, T. Tanaka, E. Bannai, and S. Kawai, J. Phys. Soc. Jpn. **42**, 112 (1977).

[8] W. Joss, J. M. van Ruitenbeek, G. W. Crabtree, J. L. Tholence, A. P. J. van Deursen, and Z. Fisk, Phys. Rev. Lett. **59**, 1609 (1987).

[9] Y. Onuki, T. Komatsubara, P. H. P. Reinders, and M. Springford, J. Phys. Soc. Jpn. **58**, 3698 (1989).

[10] H. Matsui, T. Goto, S. Kunii, and S Sakatsume, Physica B **186-188**, 126 (1993).

[11] N. Harrison, P. Meeson, P. A. Probst, and M. Springford, J. Phys.: Condens. Matter **5**, 7435 (1993).

[12] N. Sato, S. Kunii, I. Oguro, T. Komatsubara, and T. Kasuya, J. Phys. Soc. Jpn. **63**, 3967 (1984).
[13] M. Biasini, M. A. Alam, H. Harima, Y. Onuki, H. M. Fretwell, and R. N. West, J. Phys.: Condens. Matter **6**, 7823 (1994).
[14] S. Tanigawa, S. Terakado, K. Ito, A. Morisue, T. Komatsubara, and Y. Onuki, *Positron Annihilation*, edited by P. C. Jain, R. M. Singru, and K. P. Gopinatan (World Scientific, Singapore, 1985), p. 285.
[15] S. Tanigawa, T. Kurihara, M. Osawa, T. Komatsubara, and Y. Onuki, *Positron Annihilation*, edited by L. Doriken-Vanpraet, M. Doriken, and D. Seegers (World Scientific, Singapore, 1988), p. 239.
[16] D. G. Lock, V. H. Crisp, and R. N. West, J. Phys. F **3**, 561 (1973).
[17] N. Shiotani, Solid State Phys. (Tokyo) **19**, 526 (1984).
[18] S. Berko, *Positron Solid State Physics*, edited by W. Brandt and A. Dupasquier (North-Holland, Amsterdam, 1983), p. 64.
[19] R. N. West, J. Mayers, and P. A. Walters, J. Phys. E **14**, 478 (1979).
[20] A. Hasegawa and A. Yanase, J. Phys. F **7**, 1245 (1977).
[21] H. Harima, O. Sakai, T. Kasuya, and A. Yanase, Solid State Commun. **66**, 603 (1988).
[22] H. Haghighi, J. H. Kaiser, S. Rayner, R. N. West, J. Z. Liu, R. Shelton, R. H. Howell, F. Solal, and M. J. Fluss, Phys. Rev. Lett. **67**, 382 (1991).
[23] Y. Kubo and S. Asano, Phys. Rev. B **39**, 8822 (1989).
[24] Y. Kubo, Proc. Inst. Nat. Sci. **28**, 121 (1993).
[25] Y. Kubo and S. Asano, J. Magn. Magn. Mater. **104-107**, 1182 (1992).
[26] A. B. Andrews, J. J. Joyce, A. J. Arko, J. D. Thompson, J. Tang, J. M. Lawrence, and J. C. Hemminger, Phys. Rev. B **51**, 3277 (1995).
[27] J. J. Joyce, A. J. Arko, A. B. Andrews, R. I. R Blith, R. J. Bartlett, J. D. Thompson, Z. Fisk, P. S. Riseborough, P. C. Canfield, C. G. Olson, and P. J. Benning, Physica B **205**, 365 (1995).
[28] T. Jarlborg and A. K. Singh, Phys. Rev. B **36**, 4660 (1987).
[29] M. Kitamura, Phys. Rev. B **49**, 1564 (1994).
[30] A further comparative analysis of the CeB_6 (100) and (110) projections, described in M. Biasini, Ph.D. Thesis, Bristol, 1996, supports this conjecture.
[31] T. Chiba (private communication).
[32] A. Manuel (private communication).